JOURNAL OF GEOPHYSICAL RESEARCH, VOL. 106, NO. D18, PAGES 20,767–20,782, SEPTEMBER 27, 2001

Regional physical and chemical properties of the marine boundary layer aerosol across the Atlantic during Aerosols99: An overview

Timothy S. Bates,[1,2,3] Patricia K. Quinn,[1,2] Derek J. Coffman,[2,1] James E. Johnson,[2,1] Theresa L. Miller,[2,1] David S. Covert,[3,2] Alfred Wiedensohler,[4] Stephan Leinert,[4] Andreas Nowak,[4] and Christian Neusüss[4]

Abstract. The Aerosols99 cruise crossed the Atlantic Ocean from Norfolk, Virginia, to Cape Town, South Africa, between January 14 and February 8, 1999. The goals of the cruise were to determine the chemical, physical, and optical properties of the marine boundary layer (MBL) aerosol, the vertical distribution of aerosols and ozone, the column-integrated aerosol optical depth, and the ozone, CO, and peroxy radical chemistry in the MBL. Sampling strategies were optimized to obtain data sets to evaluate satellite-derived ocean color (Sea-viewing Wide Field-of-view Sensor), aerosol optical depth (advanced very high resolution radiometer) and total column ozone (Total Ozone Mapping Spectrometer). The cruise track crossed through seven different meteorological/oceanographic regimes ranging from background marine air masses in the Northern and Southern Hemispheres to air masses containing mineral dust and the products of biomass burning. This overview discusses the seven regimes encountered enroute and the chemical and physical properties of the MBL aerosol in each regime.

1. Introduction

The large uncertainties in the tropospheric distributions of short-lived chemical species, primarily aerosols and ozone, limit our ability to accurately calculate radiative forcing of climate [*Intergovernmental Panel on Climate Change (IPCC)*, 1996]. These uncertainties are a result of the large spatial and temporal variability that results from widely dispersed sources and relatively short (as compared to most green house gases) lifetimes. A better understanding of the regional and temporal variations in these distributions and the processes controlling them is fundamental to improving climate models.

Satellite observations are providing increasingly better global views of aerosol [*King et al.*, 1999] and ozone [*Fishman and Brackett*, 1997; *Thompson and Hudson*, 1999] distributions. However, the conversion of satellite radiances to aerosol and ozone distributions requires a large number of assumptions [*Kiehl et al.*, 1999; *King et al.*, 1999]. Although in situ observations cannot achieve the spatial and temporal coverage provided by satellites, they provide detailed and accurate aerosol chemical, physical, and optical data and ozone vertical profiles that can play a crucial role in constraining, developing, testing, and validating chemical transport and radiative transfer models and satellite retrieval algorithms. Clearly, a combined approach of in situ measurements, satellite observations, and atmospheric chemistry models is required to produce the needed chemical distributions.

Research ship cruises provide a means by which to acquire comprehensive in situ and column-integrated data over a large geographical area. The Aerosols99 cruise was designed to quantify the short-lived chemical species (gases and aerosols) over the Atlantic Ocean. Although most of the measurements were confined to the marine boundary layer (MBL), radiosondes, ozonesondes, lidars, and sunphotometers provided information on the vertical distribution of ozone and aerosols. The cruise departed Norfolk, Virginia, on January 14, 1999, and arrived in Cape Town, South Africa, on February 8, 1999 (Figure 1). Air masses encountered enroute included the following: a continental North American plume, a background North Atlantic air mass, mineral dust from North Africa, biomass burning from North Africa, and background South Atlantic air masses.

[1]Pacific Marine Environmental Laboratory, NOAA, Seattle, Washington.
[2]Joint Institute for the Study of the Atmosphere and Ocean, University of Washington, Seattle, Washington.
[3]Department of Atmospheric Sciences, University of Washington, Seattle, Washington.
[4]Institute for Tropospheric Research, Leipzig, Germany.

Paper number 2000JD900578.
0148-0227/01/2000JD900578$09.00

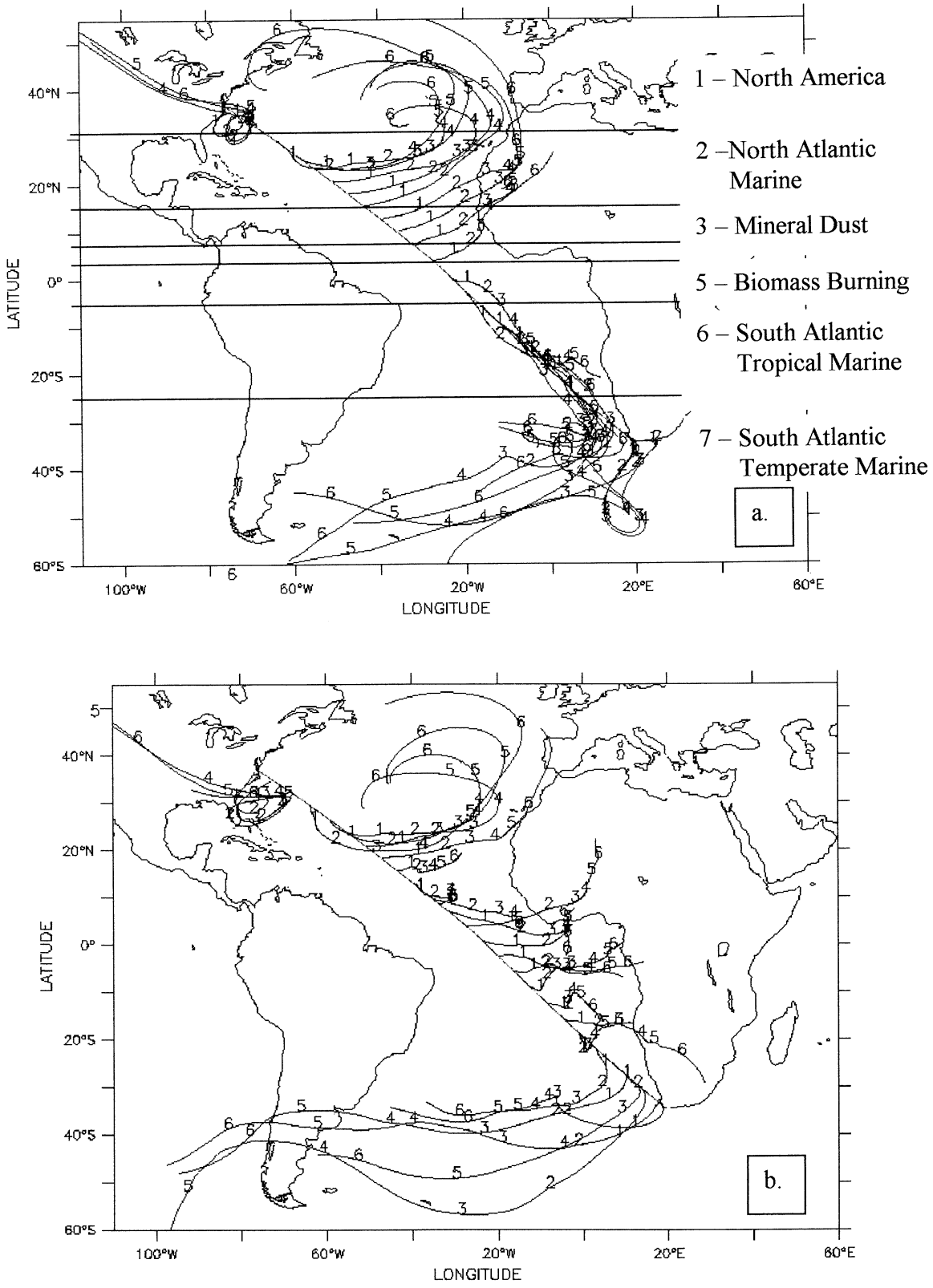

Figure 1. (a) Six-day 3-D air mass back trajectories arriving at a height of 950 mbar above the ship daily at 0000 UT. The seven air mass regimes sampled along the cruise track are delineated by the horizontal lines. Note region 4 (3°N to 5°S) was a mixture of mineral dust (region 3) and biomass burning (region 5). (b) Six-day 3-D air mass back trajectories arriving at a height of 750 mbar above the ship daily at 0000 UT. Numbers indicate the days back from the ship position.

This manuscript provides an overview of the oceanic and meteorological regimes encountered enroute as well as a description of the chemical and physical aerosol properties. Further details on the aerosol chemical mass closure (S. Leinert et al., unpublished manuscript, 2000), aerosol components and their affect on the aerosol optical properties [*Quinn et al.*, this issue], aerosol hygroscopic properties (A. Massling et al., unpublished manuscript, 2000), aerosol vertical structure and optical depth [*Voss et al.*, this issue (a and b)], regional aerosol properties (P. Durkee et al., unpublished manuscript, 2000), ocean color (R. Frouin et al., unpublished manuscript, 2000), MBL photochemistry, and peroxy radical chemistry [*Andrés Hernández et al.*, this issue] can be found in this special section. The MBL and vertical distributions of ozone along the cruise track were described previously by *Thompson et al.* [2000].

2. Oceanographic and Meteorological Overview Along the Aerosols99 Cruise Track

2.1. Oceanographic Regimes

The Aerosols99 cruise passed through several distinct water masses that are evident in the upper water column salinity and temperature distributions (not shown)

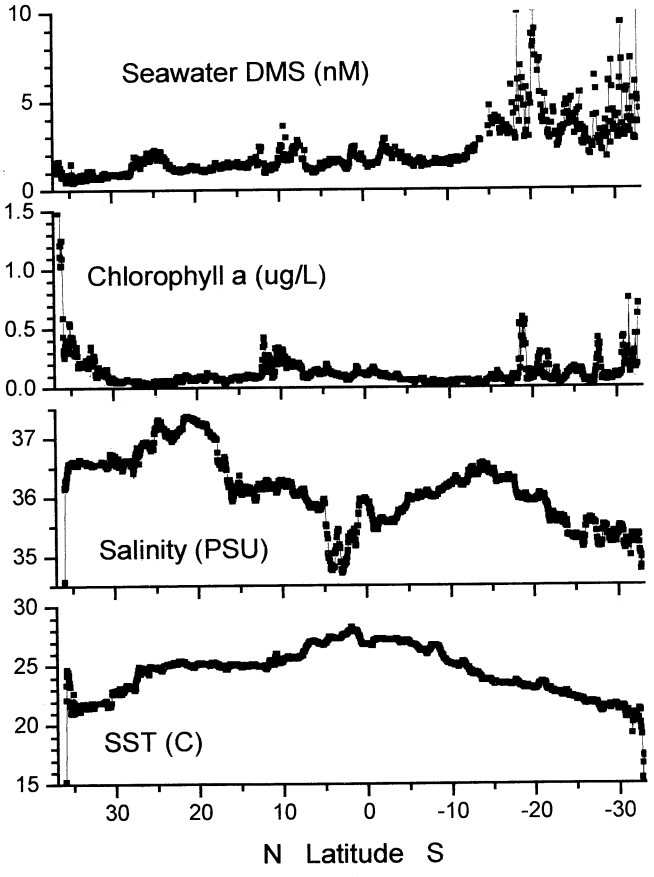

Figure 2. Thirty-minute averages of surface seawater temperature, salinity, chlorophyll a, and DMS along the Aerosols99 cruise track.

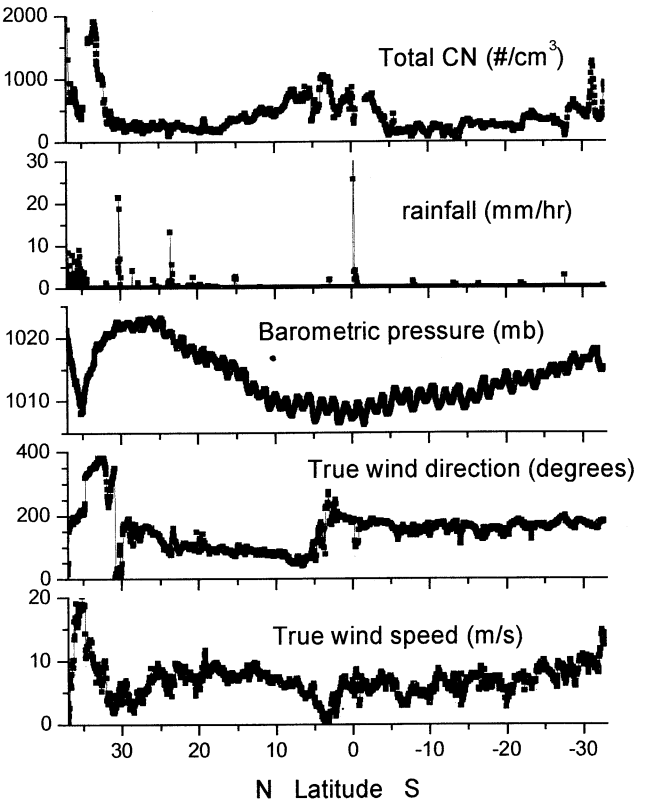

Figure 3. Thirty-minute average true wind speed, true wind direction, barometric pressure, rainfall rate, and total particle number (as measured with a TSI 3010) along the Aerosols99 cruise track.

and the surface seawater temperature (SST) and salinity data (Figure 2). The ship left the colder, nutrient-rich (nitrate plus nitrite concentrations up to 2 μM) coastal waters at 36°N and crossed through the warm Gulf Stream waters between 36° and 35°N. Surface seawater nitrate plus nitrite concentrations dropped below detection limit (0.05 μM), and chlorophyll "a" concentrations dropped to less than 0.1 μg/L in the waters between the Gulf Stream and warmer, more saline Sargasso Sea beginning at 30°N (Figure 2). Salinity concentrations decreased rapidly on the southern edge of the Sargasso Sea at 20°N–15°N. Chlorophyll concentrations were variable between 0.05 and 0.43 μg/L in the North Equatorial Current between 15°N and 8°N; however, nitrate concentrations never rose above the detection limit for the remainder of the cruise. SST increased, and salinity values began to decrease at the northern edge (8°N) of the Intertropical Convergence Zone (ITCZ). Between 5°N and the equator, salinity values decreased markedly to 34.8 practical salinity units (psu). Surface wind speed and direction abruptly changed in this region (Figure 3). There was no evidence of upwelling at the equator in the subsurface temperature and salinity distributions. The mixed layer depth at the equator was 50–60 m deep. South of the equator the ship crossed the South Equatorial Cur-

rent into the anticlyclonic gyre of the South Atlantic where salinity values increased and chlorophyll concentrations again decreased. On the southeastern side of the gyre (approximately 15°S), salinity and temperature values decreased, and chlorophyll concentrations increased (Figure 2) from the influence of the Benguela Current.

2.2. Meteorological Regimes

This meteorological overview and the delineation of seven distinct MBL air mass regimes along the cruise track are based on the meteorological data, calculated back trajectories, trace gas distributions, and aerosol chemical and physical data. The aerosol chemical constituents, in particular, are excellent tracers for defining the recent history of the air mass. The specific properties of the aerosol data in these regions will be discussed in detail in sections 4–6. The air mass regimes defined here are not necessarily consistent with the overlying free troposphere where layers of enhanced ozone [*Thompson et al.*, 2000] and/or aerosol [*Voss et al.*, this issue (a)] concentrations may have advected to the region from different source regions.

2.2.1. Region 1: 37°N–31°N, North American air mass. Leaving Norfolk, the ship was initially under the influence of a small low-pressure system that passed north of the ship bringing high winds (20 m s^{-1}) and rainfall (Figure 3). The surface barometric pressure began rising, and the wind direction shifted to the north as the ship passed 35°N (Figure 3). The wind speed dropped dramatically (20 m s^{-1} to 2 m s^{-1}) between 35°N and 31°N as the ship came under the influence of a small high-pressure system. Six day isentropic back trajectories (Figure 1) showed that the MBL air mass sampled at the ship between 35°N and 31°N had rapidly crossed North America on the back side of a large low-pressure system centered over Canada and then followed the anticyclonic flow over the western Atlantic Ocean for several days. (The top of the MBL is defined as the top of the lowest cloud-containing layer or, in the case of cloud-free conditions, the level where the relative humidity (RH) rapidly decreases and is based on soundings every 12 hours.)

2.2.2. Region 2: 31°N to 15.5°N, North Atlantic marine air mass. At 31°N the ship came under the influence of the Azores High. The subsiding air masses reaching the ship had been over the Atlantic Ocean for more than 6 days (Figure 1a). MBL heights ranged from 1.5 to 2.5 km (Figure 4) except during a 1.5 day period (between 29.5°N and 25°N) when an easterly wave within the trade winds mixed the moist MBL air to 7 km (Figure 4). Calculated 6 day back trajectories (2500 m shown in Figure 1b and 5000 m, not shown) showed that the upper level air had also been confined to the North Atlantic during this time. On the basis of lidar data the atmospheric aerosol was largely confined to the MBL [*Voss et al.*, this issue (a)].

2.2.3. Region 3: 15.5°N to 8°N, African dust air mass. At 15.5°N the MBL anticyclonic flow around the Azores High that reached the ship had

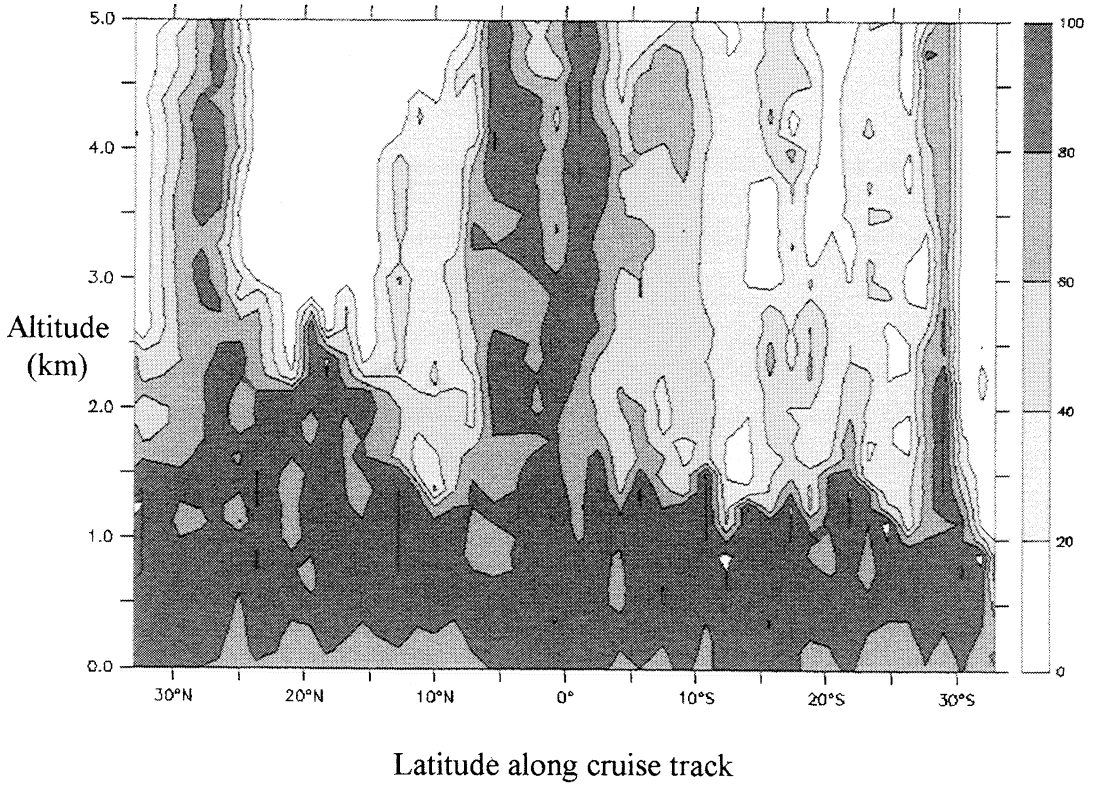

Figure 4. Relative humidity profiles from the radiosondes launched along the Aerosols99 cruise track.

crossed northwest Africa (Figure 1) bringing an aerosol with the chemical signature of mineral dust. The upper level flow at this point was quite weak (Figure 1b), and the MBL decreased to 1.3 km. Enhanced (up to a factor of 10 times higher than marine background values) aerosol optical depths in regions 3 and 4 also were clearly apparent in the high-resolution advanced very high resolution radiometer (AVHRR) satellite data and Sun photometer data collected aboard the ship [*Voss et al.*, this issue (b), P. Durkee et al., unpublished manuscript, 2000]. The lidar data showed two distinct aerosol layers with a distinct extinction minimum between them [*Voss et al.*, this issue (a)]. The MBL aerosol accounted for approximately $\frac{3}{4}$ of the aerosol optical depth (AOD), while the upper layer aerosol, centered at an altitude of approximately 2 km, accounted for the remaining $\frac{1}{4}$ [*Voss et al.*, this issue (a)].

2.2.4. Region 4: 8°N to 3°N, mixed African dust and biomass burning in the ITCZ. At 8°N the ship entered the ITCZ where the surface wind speed decreased from 6 m s^{-1} to less than 1 m s^{-1} and the wind direction changed from the northeast to the southeast. There was no well-defined MBL as the lower atmosphere was moist and convective to 7 km (shown to 5 km in Figure 4). Calculated back trajectories at the surface continued to cross North Africa bringing a chemical signature of mineral dust. Calculated 6-day upper level (750 mbar) trajectories (Figure 1b), still within the moist mixed layer, crossed southwestern North Africa bringing a chemical signature of biomass burning to the lower MBL at the ship. Lidar-derived aerosol extinction extended to 4 km but with less distinct aerosol layering than that observed in region 3 [*Voss et al.*, this issue (a)].

2.2.5. Region 5: 3°N to 5°S, biomass burning in the ITCZ. At 3°N the southeast winds began to increase in speed (Figure 3), and MBL ozone concentrations began to decrease. The lower atmosphere remained moist and convective to 7 km. Calculated back trajectories at the surface were now being steered by the subtropical high of the South Atlantic, and the mineral dust chemical signature was no longer present in aerosol samples collected on the ship. Calculated 6-day upper level back trajectories (2500 and 5500 m) continued to cross southwestern North Africa bringing aerosols to the lower marine boundary layer with a chemical signature of biomass burning. Significant aerosol extinction again extended to 4 km [*Voss et al.*, this issue (a)].

2.2.6. Region 6: 5°S to 24.5°S, South Atlantic tropical marine air mass. At 5°S, surface ozone and CO concentrations [*Thompson et al.*, 2000] had reached Southern Hemisphere background levels. Total particle number decreased from an average of 620 ± 200 cm^{-3} in the ITCZ to 230 ± 83 cm^{-3} in region 6 (Figure 3). The MBL was again capped at 1.2 to1.5 km (Figure 4), and MBL 6-day back trajectories remained over the ocean. Upper layer 6-day back trajectories either remained over the ocean or extended over South Africa. An aerosol layer above the MBL persisted to 12°S [*Voss et al.*, this issue (a)], but appeared to have little affect on the gas or aerosol chemistry of the MBL.

2.2.7. Region 7: 24.5°S to 33°S, South Atlantic temperate marine air mass. At approximately 24.5°S the MBL and upper level 6-day back trajectories became longer and extended across the South Atlantic (Figure 1). The MBL height ranged from 1.2 to 1.5 km except in the region between 28°S and 30°S where the moist surface layer was mixed to >11 km as a result of a low-pressure system south of South Africa. Surface wind speeds increased from an average trade wind speed of 6.0 ± 1.3 m s^{-1} in region 6 to 9.1 ± 1.8 m s^{-1} in region 7 (Figure 3).

3. Methods

3.1. Inlet

Aerosol sampling and analysis methods were similar to those used in the First Aerosol Characterization Experiment (ACE 1) [*Bates et al.*, 1998a, b; *Quinn et al.*, 1998] and ACE 2 [*Bates et al.*, 2000; *Quinn et al.*, 2000]. Aerosol particles were sampled 18 m above the sea surface through a heated mast that extended 5 m above the aerosol measurement container. The mast was capped with a cone-shaped inlet nozzle that was rotated into the relative wind to maintain nominally isokinetic flow and minimize the loss of supermicron particles. Air was drawn through the 5 cm diameter inlet nozzle at 1 m^3 min^{-1} and down the 20 cm diameter mast. The lower 1.5 m of the mast were heated to dry the aerosol to a relative humidity (RH) of 55 ± 5%. This allowed for constant instrumental size cuts through variations in ambient RH. Fifteen 1.9 cm diameter electrically conductive polyethylene or stainless-steel tubes extend into this heated zone to direct the airstream at flows of 30 L min^{-1} to the various aerosol sizing/counting instruments and impactors. Comparisons of the total particle count (Dp > 3 nm) during intercomparisons with the National Center for Atmospheric Research (NCAR) C-130 airplane and ACE 1 ground stations agreed to within 20%, suggesting minimal loss of particle number in the inlet system [*Weber et al.*, 1999]. A similar comparison with the NCAR C-130 during the Indian Ocean Experiment (INDOEX) showed agreement to within 5%. Assessing the inlet efficiency for larger particles is more difficult. Comparisons of marine boundary layer particle extinction based on in situ measurements and total column measurements (NASA Ames suntracking sunphotometer, *Livingston et al.* [2000]) during ACE 2 agreed to within the uncertainties of the measurements and calculations; however, those uncertainties are quite high.

3.2. Aerosol Number Distributions and Concentrations

Total particle number concentrations were measured with Thermo Systems Inc. (TSI) 3010 and TSI 3025 particle counters (CPC) operated directly off one of the

1.9 cm sampling tubes and a TSI 3010 particle counter connected to an independent 0.6 cm sampling line running to the top of the sampling mast. The 30-min averaged data over the length of the cruise from the two TSI 3010 counters agreed to within 3.6 ± 9.5% (mean plus or minus one standard deviation of the ratio). The 30-min average data from the TSI 3025 particle counter was on average 16 ± 6.8% higher than the data from the TSI 3010 counters.

One of the fifteen 1.9 cm diameter tubes was used to supply ambient air to a differential mobility particle sizer (DMPS) located inside the humidity-controlled box at the base of the mast. The DMPS was a University of Vienna (Reischle) medium column, operating with a negative particle charge, connected to a TSI 3010 particle counter. Data were collected in 27 size bins between 22 and 900 nm diameter. The DMPS operated with an aerosol flow rate of 0.5 L/min and a sheath air flow rate of 5 L/min. The sheath air was humidified to 55% RH. Another one of the 1.9 cm diameter tubes was used to supply ambient air to an ultrafine differential mobility particle sizer (UDMPS) and DMPS located just outside the humidity-controlled box at the base of the mast. The UDMPS was a University of Vienna (Reischle) short-column instrument, operating with a negative particle charge, connected to a TSI 3025 particle counter. Data were collected in 14 size bins between 3 and 22 nm diameter. The UDMPS operated with an aerosol flow rate of 1 L/min and a sheath airflow rate of 10 L/min. The DMPS on this inlet was identical to the one in the humidity-controlled box. However, the relative humidity of the sheath air was dry resulting in a measurement RH in the UDMPS/DMPS of approximately 10%. Mobility distributions from the three systems were collected every 15-min.

The UDMPS/DMPS data were filtered to eliminate periods of calibration and instrument malfunction and periods of ship contamination (based on relative wind and high and rapid changes in condensation nuclei (CN) counts). The filtered mobility distributions were then converted to number-size distributions using the inversion routine of *Stratman and Wiedensohler* [1997]. The data were corrected for diffusional losses [*Covert et al.*, 1997] and size-dependent counting efficiencies [*Wiedensohler et al.*, 1997] based on pre-ACE 1 and ACE 2 intercalibration exercises. The accuracy of both the particle sizing and the number of particles in each size bin depends on the stability of the flow rates. Three of the four DMPS flows (CPC, Sheath, and Excess) were controlled independently in these three systems. The DMPS inlet flow was the difference of these flows, nominally 10% of the sheath flow. The flow calibration involved setting the CPC flow and differential mobility analyzer (DMA) sheath flow with an electronic bubble flowmeter. The excess flow was balanced with the sheath airflow such that the DMPS inlet flow was equal to the CPC flow. The inversion and evaluation of the DMPS data assumed the sheath and excess flows were equal and that the inlet flow equaled the CPC flow. The drift in the CPC, sheath, and excess flows was generally less than 1% during the cruise (mean 0.63 ± 0.55%). This translates into a similar error in particle sizing of plus or minus a percent. However, a relative drift of 1% in the sheath to excess flow translates into a 10% change in the DMPS inlet flow and thus a 10% change in the number concentration. A change in the inlet flow also results in a change in the transfer function of the DMA which compounds this error; for example, for this case the combined error is of the order of 15%. During Aerosols99 the integrated number concentration from the DMPS operated at 55% RH averaged 18 ± 10% lower than the total number measured by the TSI 3010. The integrated number concentration from the DMPS system operated at 10% RH averaged 21 ± 6% lower than the total number measured by the TSI 3010. To correct for the number concentration error, the DMPS data reported have been normalized using the 30-min average ratio of the total number concentration to the integrated DMPS number concentration. An interactive routine was then used to fit lognormal curves to the different modes of the DMPS number size distributions.

Another one of the 1.9 cm tubes was connected to an Aerodynamic Particle Sizer (APS, TSI 3320) located in the humidity-controlled box at the base of the mast. The APS measured the number size distribution between 0.6 and 9.6 μm aerodynamic diameter. Data at diameters larger than 5 μm were discarded due to potential interferences from phantom counts and uncertainties in large particle collection efficiencies. Although the intent was to measure this distribution at 55% RH, the heat from the instrument effectively dried the sea-salt aerosol to below its efflorescence point.

3.3. Aerosol Chemistry

Detailed descriptions of the aerosol chemical measurements, data reduction, and uncertainties are presented by *Quinn et al.* [this issue]. A brief description of the measurements is presented below.

Two-stage multijet cascade impactors [*Berner et al.*, 1979] sampling air at 55% RH were used to determine the submicron and supermicron concentrations of Cl^-, NO_3^-, $SO_4^=$, methanesulfonate (MSA^-), Na^+, NH_4^+, K^+, Mg^{+2}, and Ca^{+2}. The RH of the sampled airstream was measured a few inches upstream from the impactor. The 50% aerodynamic cutoff diameters $D_{50,\mathrm{aero}}$ were 1.1 and 10 μm. Throughout the paper, submicron refers to particles with $D_{\mathrm{aero}} < 1.1$ μm at 55% RH, and supermicron refers to particles with 1.1 μm $< D_{\mathrm{aero}} < 10$ μm at 55% RH.

Non-sea-salt sulfate concentrations were calculated from Na^+ concentrations and the ratio of sulfate to sodium in seawater. Sea-salt aerosol concentrations were calculated as

$$\begin{aligned}\text{sea salt } (\mu\text{g m}^{-3}) = {} & \mathrm{Cl}^-(\mu\text{g m}^{-3}) \\ & + \mathrm{Na}^+ (\mu\text{g m}^{-3}) \times 1.47,\end{aligned} \quad (1)$$

where 1.47 is the seawater ratio of ($Na^+ + K^+ + Mg^{+2} + Ca^{+2} + SO_4^{=} + HCO_3^-$)/$Na^+$. This approach prevents the inclusion of non-sea-salt K^+, Mg^{+2}, Ca^{+2}, $SO_4^{=}$, and HCO_3^- in the sea-salt mass and allows for the loss of Cl^- mass through Cl^- depletion processes. It also assumes that all measured Na^+ and Cl^- is derived from seawater.

Three-stage multijet cascade impactors [*Berner et al.*, 1979] sampling air at 55% RH were used to determine submicron and supermicron concentrations of total carbon (TC), organic carbon (OC), and elemental carbon (EC). The impactor had $D_{50,aero}$ of 0.18, 1.1, and 10 μm. Only in this case does submicron refer to $0.18 < D_{aero} < 1.1$ μm. The 0.18 μm jet plate was used instead of a quartz backup filter to minimize positive artifacts due to the absorption of gas phase organics. The samples were analyzed by a thermographic method using a commercial instrument (C-mat 5500, Ströhlein) [*Neusüss et al.*, 2000]. As with all thermal carbon measurements, the OC/EC split is a method-dependent property. No attempt was made to correct for positive or negative sampling artifacts since the information to do so was not available.

The mass of particulate organic matter (POM) was determined by multiplying the measured OC concentration in μg C m^{-3} by a POM factor which is an estimated average of the molecular weight per carbon weight for the organic aerosol [*Turpin et al.*, 1994, 2000]. On the basis of a review of published measurements a value of 1.6 was used for the North American air masses, and a value of 2.1 was used for all other air mass regions.

Total elemental composition (Na, Mg, Al, Si, P, Cl, K, Ca, Ti, V, Cr, Mn, Fe, Ni, Cu, Zn, Ba, As, and Pb) was determined by thin-film X-ray primary- and secondary-emission spectrometry [*Feely et al.*, 1991, 1998]. Submicron samples were collected on Nuclepore filters (0.4 μm pore size) mounted in a Berner impactor downstream of the $D_{50,aero}$ 1.1 μm jet plate. Bulk samples were collected on Nuclepore filters (0.4 μm pore size) in a filter pack having an upper $D_{50,aero}$ of 10 μm. Supermicron elemental concentrations were determined by difference between the submicron and bulk samples. This method of sample collection allows for the sharp size cut of the impactor while collecting a thin film of aerosol necessary for the X-ray analysis.

For the regions of African dust and the dust/biomass burning mixture, dust concentrations were calculated from the Al mass concentration and an assumed Saharan dust to Al mass ratio of 12.5. This is based on the relatively constant 8% mass fraction of Al found in continental soils including Saharan dust (D. Savoie, personal communication, 2000). Outside of these regions the concentrations of all elements measured by XRF were summed to create a "trace element" component mass concentration. Since the molecular form of the elements was not determined, the summed concentrations do not include any associated mass (e.g., the oxygen associated with aluminum oxide).

3.4. Additional Measurements

Additional measurements made aboard the ship, that are used in the analysis below, include atmospheric and seawater dimethylsulfide (DMS) [*Bates et al.*, 1998b, 2000], atmospheric temperature, pressure, and humidity, surface seawater temperature, salinity, chlorophyll and nitrate concentrations, wind speed and direction, rainfall rates, solar radiation, and vertical profiles of temperature, dew point temperature, and wind speed and direction from radiosondes. Three-dimensional (3-D) air mass back trajectories were calculated four times daily at three altitudes using the Hybrid Single-Particle Lagrangian Integrated Trajectory (HY-SPLIT 4) model [*Draxler*, 1992] which is based on the National Centers for Environmental Prediction (NCEP) wind fields. All references to time are reported here in UTC. Dates are given as day of year (DOY) where noon on February 1 is equal to DOY 32.5.

4. MBL Aerosols Derived From Marine Sources

4.1. Sea-Salt Particles

The ocean is a direct source of aerosols to the atmosphere as a result of turbulence at the ocean-atmosphere interface. These directly emitted aerosols are primarily sea salt and were the dominant component of the aerosol mass in all regions except in the African dust air mass (Figure 5). The consistency of the soluble Mg^{2+}/Na^+ molar ratio along the cruise track (0.11 $\pm$ 0.007), and the agreement of this value with that found in sea salt (0.12), suggest that continental sources of soluble Mg^{2+} and Na^+ were insignificant. Average regional submicron and supermicron sea-salt concentrations ranged from 0.08 to 0.39 μg m^{-3} and 4.6 to 19 μg m^{-3}, respectively (Figure 5 [see also *Quinn et al.*, this issue]). The MBL concentrations are a function of wind speed and fetch (source), MBL height (vertical mixing), and wet and dry deposition (sink). The lowest concentrations were measured in the biomass burning air mass (3°N to 5°S) due to the initially low wind speeds (Figure 3), convective mixing (Figure 4), and heavy rainfall (Figure 3). The highest concentrations were measured in the African dust air mass (15.5°N to 8°N) due to the low and stable MBL.

Although the relative abundance of the sea-salt ions initially emitted into the atmosphere is the same as that found dissolved in surface seawater, reactions with acidic gases and condensed phase compounds in the atmosphere can lead to depletion of the halide concentrations [*Chameides and Stelson*, 1992; *Posfai et al.*, 1995; *Keene and Savoie*, 1998]. Submicron and supermicron sea-salt particles were depleted in chlorine in the North American air mass (Figure 6). This is also the region of highest sulfate and nitrate concentrations (Figure 5) which could account for the displacement of the chlorine [*Sander and Crutzen*, 1996]. The supermicron sea-salt

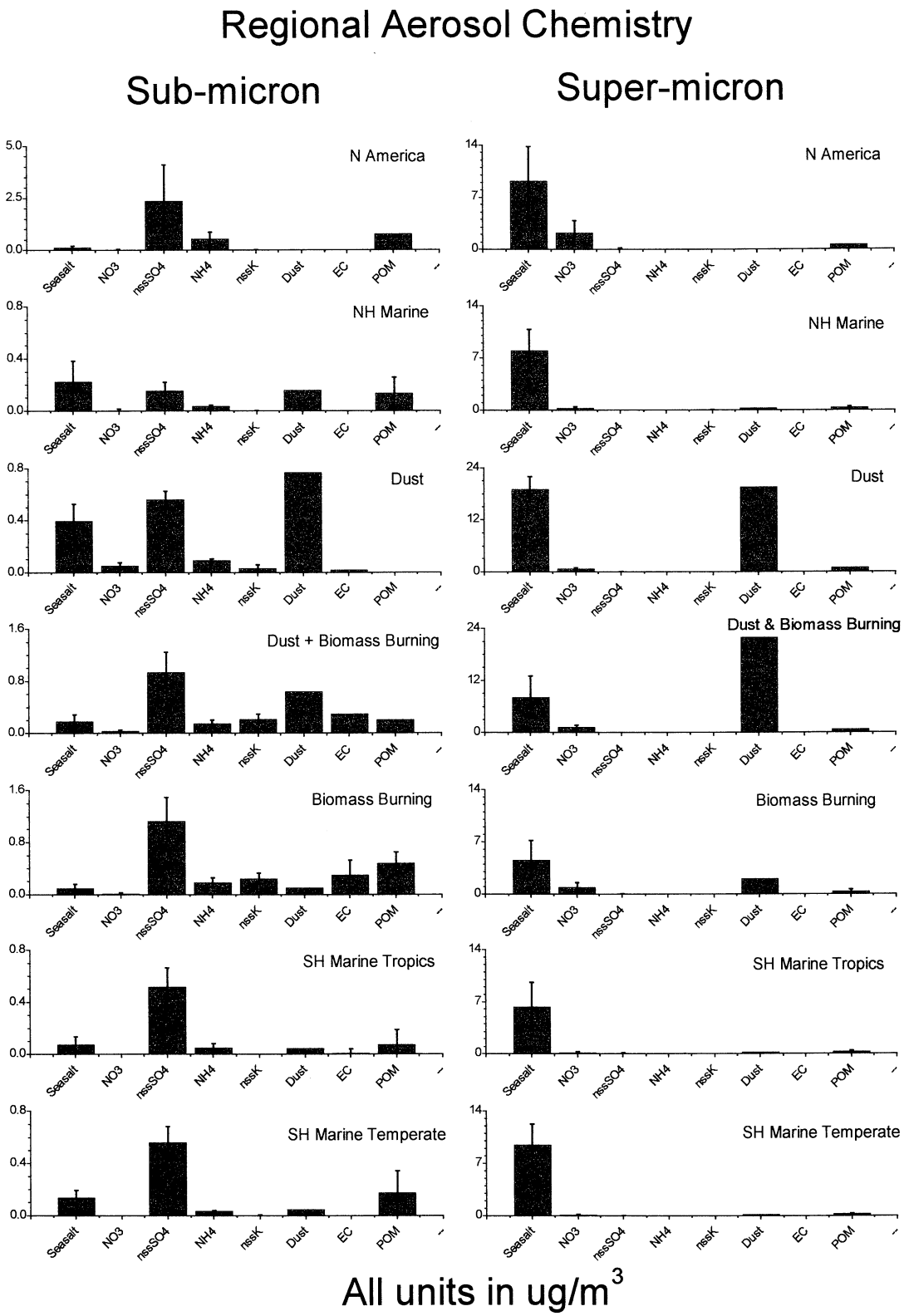

Figure 5. Submicron ($D_{\mathrm{aero}} < 1.1$ μm at 55% RH) and supermicron (1.1 μm $< D_{\mathrm{aero}} < 10$ μm at 55% RH) aerosol chemistry in μg m^{-3} for the seven air mass regimes sampled along the cruise track. The error bars represent one standard deviation of the mean concentration. Absolute uncertainties are given by *Quinn et al.* [this issue]. Note that the y axis varies between regions.

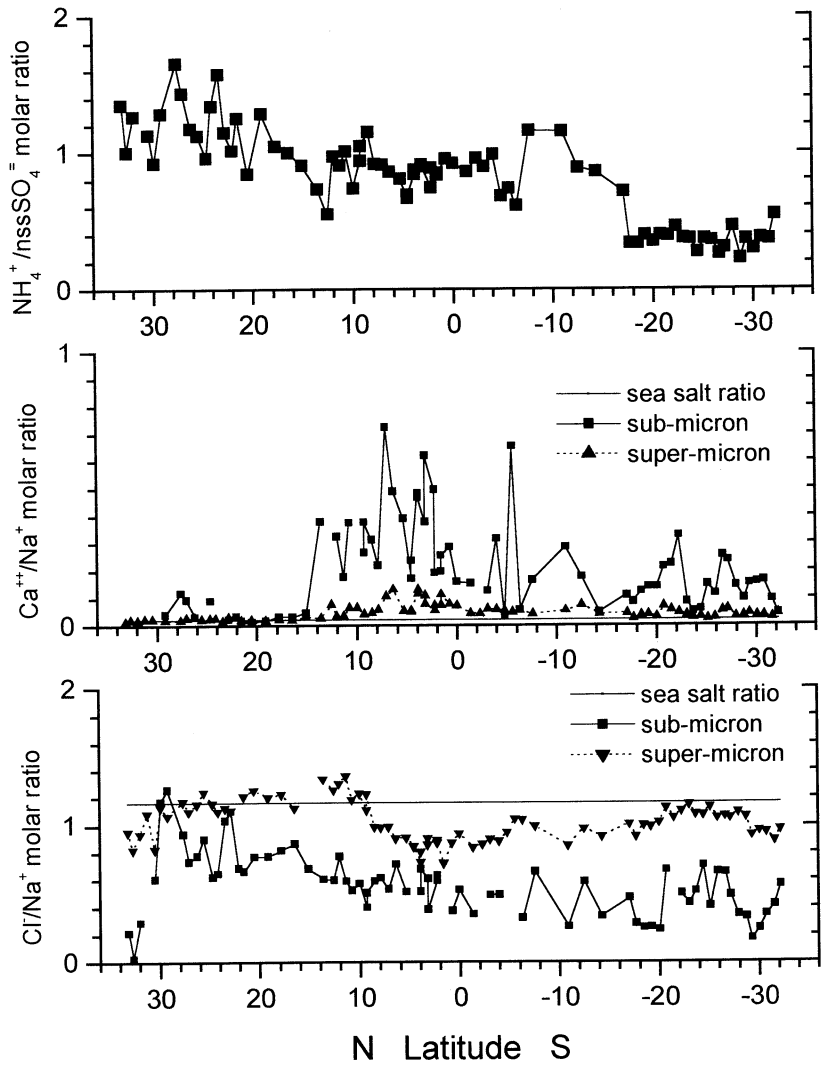

Figure 6. Molar ratios of submicron $NH_4^+/nssSO_4^=$, submicron and supermicron Ca^{++}/Na^+, and submicron and supermicron Cl^-/Na^+ measured along the cruise track. The Ca^{++}/Na^+ (0.022) and Cl^-/Na^+ (1.17) molar ratios in seawater are shown as straight lines.

particles in NH marine and dust air masses appeared to be unreacted although submicron particles were depleted in chlorine. Submicron particles continued to be depleted in chlorine in all air masses farther south. Supermicron particles were nearly unreacted in much of the SH temperate air mass. Without single particle analysis it is not possible to assess the reactions occurring on the sea-salt particles. The depletion of chlorine, however, implies that in most regions the supermicron and, especially, the submicron particles were internally mixed.

4.2. Biogenic Particles

Turbulence at the air-sea interface can also emit particles of biogenic origin into the atmosphere [*Matthias-Maser et al.*, 1999]. Average regional submicron and supermicron particulate organic matter concentrations ranged from 0.08 to 0.18 μg m^{-3} and 0.23 to 0.38 μg m^{-3}, respectively, in the NH and SH marine air masses. In the SH, calcium concentrations were enriched in comparison to seawater (Figure 6), which may also be from a biogenic source. Similar calcium enhancements have been previously reported [*Cattell et al.*, 1977; *Sievering et al.*, 1999]. Without details on the molecular composition of these particles or visual identification via electron microscopy, it is not possible to confirm the source of this material. Alternatively, this material may have come from continental sources via long-range transport in the MBL (>6 days) or subsidence from the free troposphere.

4.3. Non-Sea-Salt (nss) Sulfur and Ammonium-Containing Particles

Dimethylsulfide (DMS) is produced in surface seawater from the enzymatic cleavage of dimethlysulfonium propionate [*Bates et al.*, 1994]. Surface seawater DMS

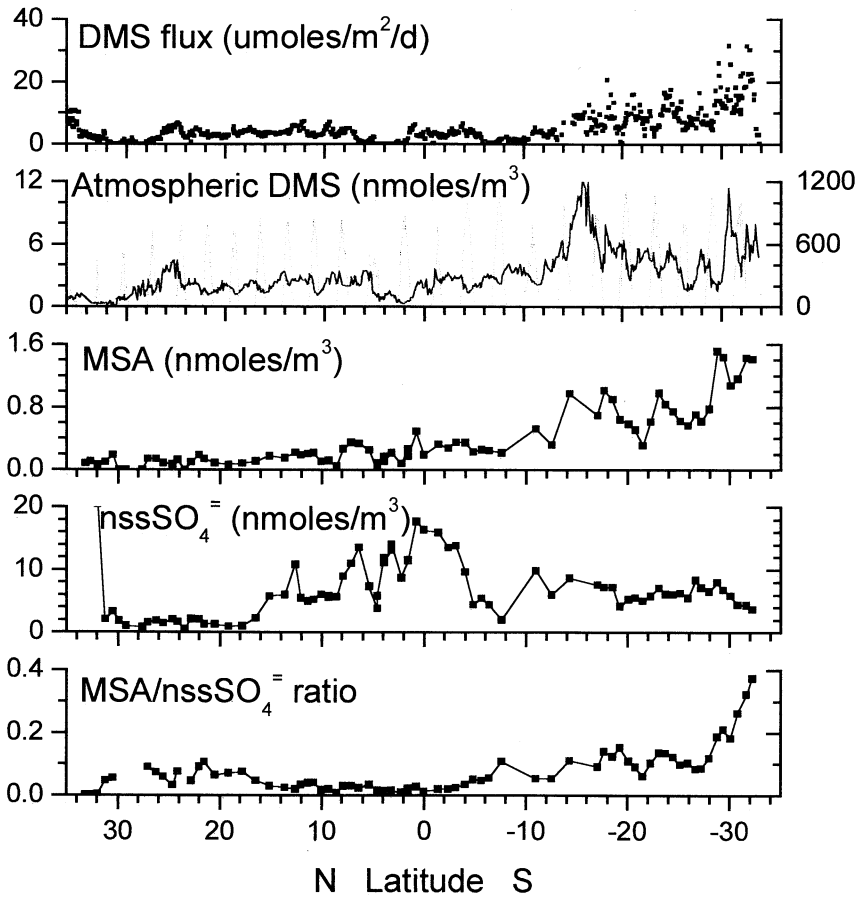

Figure 7. The calculated DMS flux, atmospheric DMS concentration, total sub-10 μm MSA and nss$SO_4^=$ concentrations, and the MSA/nss$SO_4^=$ ratio measured along the cruise track. The measured total solar insolation (W m^{-2}, right axis) is shown (dashed line) with the atmospheric DMS concentrations to illustrate the diel variation in DMS.

concentrations along the Aerosols99 cruise track ranged from 0.4 to 11 nM (Figure 2) reflecting the seasonality of DMS production [*Bates et al.*, 1987]. The highest concentrations were found south of 15°S (mean 4.1 ± 1.6 nM) in the more biologically productive waters of the Benguela Current. Similar seawater DMS concentrations were measured by *Andreae et al.* [1994] during February–March 1991 in the South Atlantic Central Gyre (1 nM) and Benguela Current (4 nM).

The production of DMS in surface seawater leads to a net flux to the atmosphere. The calculated DMS flux along the Aerosols99 cruise track, using the *Liss and Merlivat* [1986] wind speed/transfer velocity relationship, ranged from 0 to 32 μmoles m^{-2} d^{-1} (Figure 7). This flux maintained an atmospheric DMS concentration ranging from 2 to 310 ppt (0.1 to 13 nmoles m^{-3}, Figure 7). The range of concentrations and mean concentration south of 15°S (120 ± 56 ppt) was again consistent with previous measurements in this region during this season (50–300 ppt [*Andreae et al.*, 1994]; 132 ± 45 ppt [*Andreae et al.*, 1995]). A diel cycle in the atmospheric DMS concentrations was clearly evident in the background marine regions during periods when the marine boundary layer was stable (20° to 16°N, 18° to 28°S). Concentrations in the early morning were approximately a factor of 2 higher than those in the late afternoon as a result of the photochemical oxidation of DMS by OH.

Although the series of reactions and the conversion efficiencies are still a topic of debate [*Davis et al.*, 1999], some fraction of the atmospheric DMS is converted to nss sulfate and methane sulfonate (MSA) aerosol. During the Aerosols99 cruise the only evidence of newly formed particles in the MBL (a particle mode with a mean diameter less than 20 nm) occurred during the three periods of convective mixing (Figure 4) suggesting that MBL DMS did not play a major role in new particle production. DMS derived sulfur, however, can contribute to the growth of existing particles, and nss sulfate and MSA concentrations did indeed increase in the regions of enhanced DMS concentrations (Figure 7). The ratio of MSA to nss sulfate also increased at the higher southern latitudes (Figure 7) consistent with previous measurements [*Bates et al.*, 1992; *Ayers et al.*, 1996]. In the background Southern Hemisphere, 43 ± 7.3% and 92 ± 10% of the MSA and nss sulfate were present in the submicron fraction, respectively.

Ammonia is part of the biological nitrogen cycle in

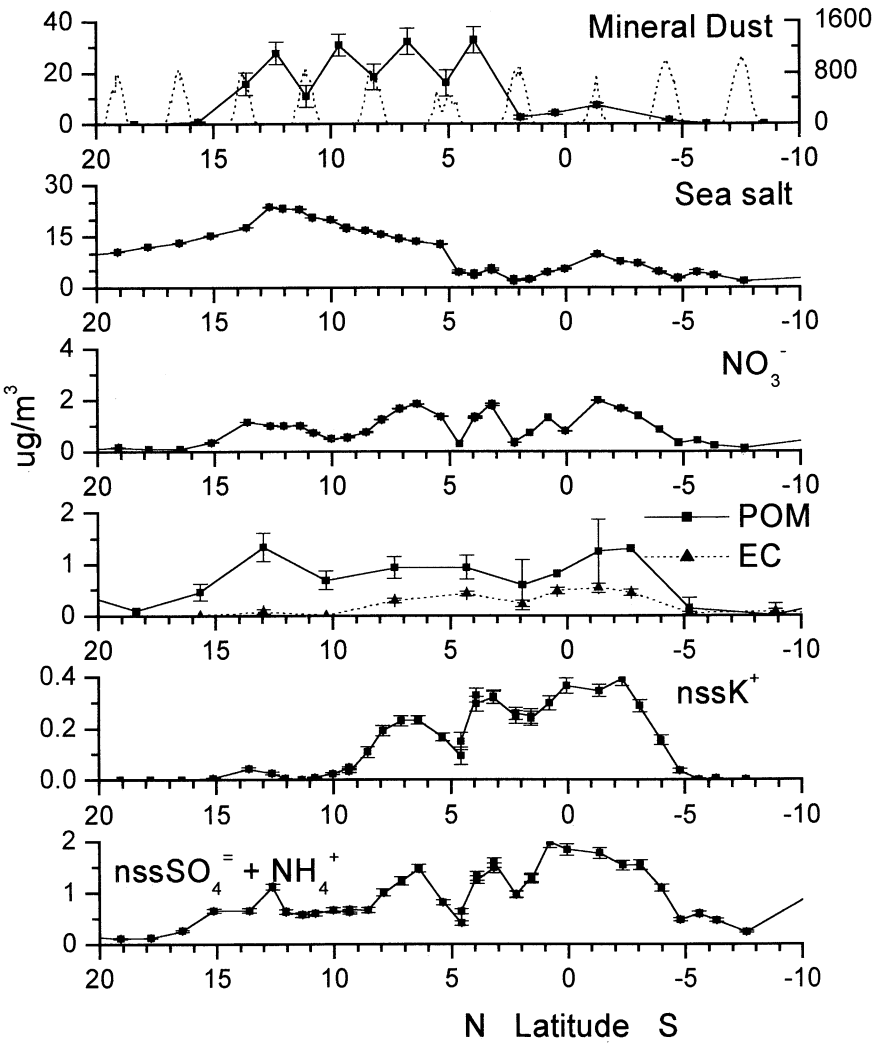

Figure 8. Total (submicron and supermicron) aerosol chemistry dominating regimes 2–6 in μg m^{-3}. The error bars show the uncertainties at the 95% confidence level [*Quinn et al.*, this issue]. The top plot also shows the measured solar insolation (dashed line) on the right axis in W m^{-2}.

the surface ocean and has a net flux to the atmosphere over the remote ocean [*Quinn et al.*, 1990; *Zhuang and Huebert*, 1996; *Gibb et al.*, 1999]. In the atmosphere, NH_3 quickly reacts with acidic aerosols. During Aerosols99, measurable ammonium (concentrations >0.001 μg m^{-3}) was present only in the submicron aerosol. The ammonium sulfate aerosol was always acidic with molar $NH_4^+/nssSO_4^=$ ratios ranging from 0.2 to 1.6 (Figure 6). The ratios dropped dramatically in the region south of 12°S where the DMS concentrations began increasing.

5. MBL Aerosols Derived From Continental Sources

Aerosols from continental sources dominated the mass distributions in four of the seven air mass regimes along the Aerosols99 Atlantic transect (Figure 5) with concentrations of nss sulfate, nitrate, and mineral dust enhanced over background marine values. There was also evidence of continental trace elements (Al, Si, shown as dust in Figure 5) in the background marine regimes, especially in the Northern Hemisphere, which may have reached the MBL through subsidence from the free troposphere. Although MBL aerosols were responsible for most of the column aerosol optical depth (35 to 95%, [*Quinn et al.*, this issue]), layers of aerosol were often apparent in the free troposphere [*Voss et al.*, this issue (a)], providing a potential aerosol source to the MBL. Some fraction of the $(NH_4)_xH_ySO_4$ and particulate organic matter also may have reached the background marine regions from the continents via long-range transport in the free troposphere [*Van Dingenen et al.*, 1995].

5.1. North American Continental Aerosols

Submicron $nssSO_4^=$ and POM and supermicron NO_3^- concentrations were highest in the North American air mass regime (Figure 5) although the limited number of samples (four inorganic ion samples, one organic and elemental sample) in this regime limits our ability to

draw any regional conclusions. This air mass also spent several days over the ocean and appeared to have been through many cloud cycles (see section 6).

5.2. North African Mineral Dust Aerosols

The mineral dust regime was clearly evident on board ship in the AVHRR satellite images (P. Durkee et al., unpublished manuscript, 2000) and visually as a red/brown deposit on the filters. The mineral dust sampled at the ship occurred in four "pulses" (Figure 8). The higher time-resolution physical parameters (aerosol scattering and coarse mode number size distribution) showed similar pulses although the magnitude of the pulses varied due to the varying sea-salt concentrations (Figure 8). The consistency of the Si/Al (3.0 ± 0.12) and Fe/Al (0.72 ± 0.064) mass ratios in the dust regions along the cruise track (15.5°N to 3°N, regimes 3 and 4) suggests a common regional source of the dust. The high Fe/Al ratio is characteristic of the ferralitic soils in the Sahelian region [*Sokolik and Toon*, 1999] that are largely mica, illite, kaolinite, and quartz [*Prospero et al.*, 1981]. The Si/Al and Fe/Al ratios measured during Aerosols99 are within the range of values given by *Bergametti et al.* [1989] for Sahelian dust source regions and are distinctly higher than that found in the northern Saharan (Moroccan) region [*Bergametti et al.*, 1989]. The calculated back trajectories cross both regions (Figure 1). The four pulses of dust observed at the ship occurred on a diel cycle with the high concentrations occurring at night and the low concentrations occurring at midday (Figure 8). No similar trend was observed in other gas or aerosol species which suggests the diel cycle was not due to changes in the mixed layer height (Figure 4) or mixing from the free troposphere. An alternate explanation could be a pulsing source term 3 to 5 days upwind of the ship (Figure 1).

Sulfate also was enriched in the mineral dust regime (Figure 8) compared to the North Atlantic marine air mass as previously reported by *Savoie et al.* [1989] and *Li-Jones and Prospero* [1998]. However, unlike the results of *Li-Jones and Prospero* [1998] which showed that most of the sulfate was present in the supermicron mode, during Aerosols99 95% of the sulfate was present in the submicron mode. This distribution suggests that the sulfate aerosol was formed prior to mixing with the dust. The presence of the sulfate in the submicron mode implies that the sulfate aerosol will have a longer lifetime with respect to dry deposition and a greater radiative impact. The ratio of nitrate to sulfate measured in the mineral dust regime during Aerosols99 (1.4) was the same as that measured by *Savoie et al.* [1989] at Barbados in December–February (1.4). On the basis of this ratio and the seasonal meteorology, *Savoie et al.* [1989] suggested sulfate and nitrate associated with the dust in the NH winter might originate from wood and biomass burning to the south of the Sahara. The low values of nss soluble potassium and elemental carbon measured in the mineral dust regime during Aerosols99, however, suggest an alternate source. Assuming tropical MSA/nss$SO_4^=$ ratio of 7% [*Saltzman et al.*, 1986], approximately 35% of this sulfur could have been derived from DMS. The remainder may have come farther upwind in the outflow from Europe. This would be consistent with the dominant submicron distribution.

5.3. North African Biomass Burning Aerosols

The southern edge of North Africa (Senegal to Ethiopia) is one of the largest fire belts observed in the world [*Gregoire et al.*, 1999]. The fire season in this region occurs during the NH winter [*Gregoire et al.*, 1999] and was active during Aerosols99 as observed by AVHRR and Total Ozone Mapping Spectrometer (TOMS) satellite imagery. The aerosols measured at the ship, beginning at the northern edge of the ITCZ (approximately 8°N), showed characteristic signals of biomass burning [*Andreae*, 1983]: elevated elemental carbon and nss K^+ concentrations (Figure 8). On the basis of the calculated back trajectories (Figure 1b) it appears that the aerosol products of biomass burning were carried to the ship at higher levels in the atmosphere (e.g., 750 mbar) and mixed down to the lower marine boundary layer in the convective ITCZ (Figure 4). The initial (8°N to 3°N) biomass burning aerosol was mixed with mineral dust. From 3°N to 5°S the mineral dust signal was minimal. Nitrate and POM concentrations were elevated throughout the dust/biomass burning region with neither region appearing to be a stronger source. Non-sea-salt sulfate and ammonia concentrations in the biomass burning region correlated well with the nss K^+ concentrations ($r^2 = 0.78$, $n = 26$) (Figure 8). KCl and NH_4Cl particles have been shown to dominate the ionic fine particles emitted from flaming fires but are converted to the sulfate salts a short distance from the fires [*Liu et al.*, 2000].

6. Comparisons of Physical Aerosol Properties Along the Aerosols99 Cruise Track

The aerosol physical properties varied widely between the seven air mass regimes (Figure 9 and Table 1). The aerosol number concentration was highest in the North American continental aerosol with a clear minimum between the Aitken and accumulation modes indicative of cloud processing [*Hoppel et al.*, 1986]. *Van Dingenen et al.* [1995] showed aerosols advecting off the continent attained the distinct two modes typical of MBL aerosol at a distance of about 1000 km and that an initially polluted continental aerosol transported in the MBL could still account for more than 50% of the aerosol volume after 5–6 days of transport time [*Van Dingenen et al.*, 2000]. On the basis of the 6-day trajectory analysis (Figure 1) the aerosols in this first Aerosols99 air mass regime had been over the ocean for 3–5 days. Comparing the sulfate concentrations in the background regime

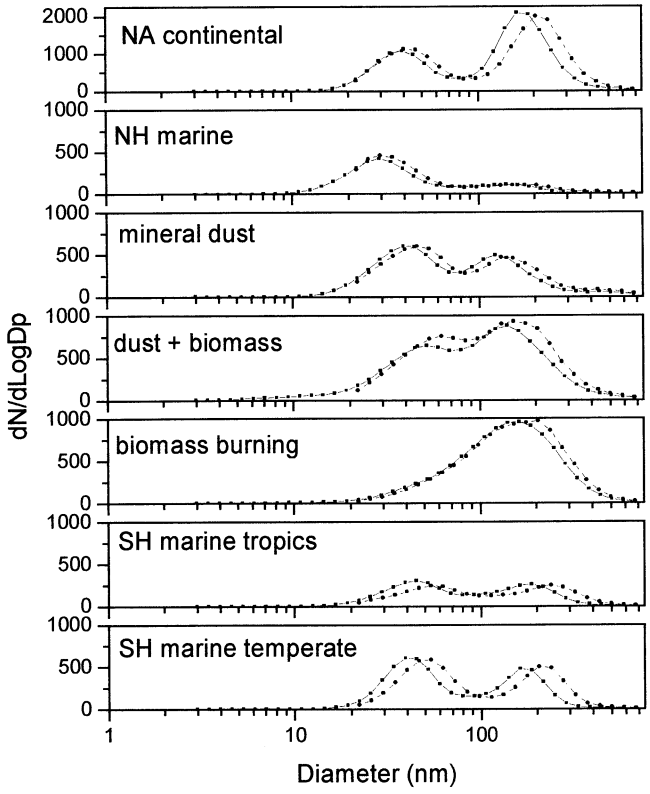

Figure 9. Regional average geometric number size distributions at <10% RH (square and solid line) and at 55% RH (dashed line) (DMPS data in $dN/d\mathrm{Log}Dp$) in the seven air mass regimes along the Aerosols99 cruise track. Note change in vertical scale for the NA continental regime.

2 with the sulfate concentrations in regime 1 suggests that the aerosol in regime 1 was still 90% continental.

The submicron aerosol measured in the North Atlantic air mass was also bimodal but with relatively small modal diameters and total numbers (Table 1). The mean modal diameters and number concentrations more closely resembled the Southern Ocean marine aerosol measured in ACE 1 than the background Atlantic aerosol measured in ACE 2 [*Bates et al.*, 2000]. The small diameters and numbers suggest recent subsidence input from the free troposphere to feed the Aitken mode [*Raes*, 1995], low MBL sulfur gas concentrations (low winter season DMS flux, both shown in Figure 7) and hence little material for condensational growth, and either a minimum of cloud processing or a short MBL residence time [*Bates et al.*, 2000]. Rain in this region (Figure 3) would suggest the latter.

The aerosol number distribution in the dust regime was dominated by the Aitken mode (Figure 9). The AVHRR satellite data show patchy cumulous clouds in the 2–3 day air mass transit from the coast to the ship that would have processed the aerosol to some degree. Comparisons of the DMPS measurements at approximately 10% and 55% RH suggest that both the Aitken and accumulation modes were composed of soluble components even though a large fraction of the submicron mass was composed of mineral dust (Figure 5). Further details of the hygroscopic properties of these aerosols are presented by A. Massling et al. (unpublished manuscript, 2000). A major feature in the size distributions in this region was the large mode in the number and volume distributions centered at 1 and 2.8 μm aerodynamic diameter, respectively (Figure 10). Most likely there are at least 2 unresolved modes within this peak from sea salt [*O'Dowd and Smith*, 1993] and mineral dust. The combination of dust and sea salt in this regime appears to shift the omni-present sea-salt mode to a lower size (Figure 10, comparison of supermicron mode in different regimes).

The submicron aerosol in the biomass burning regime was dominated by the accumulation mode (Figure 9) which is typical of a well-aged continental aerosol with high source region concentrations and dry transport conditions [*Bates et al.*, 2000]. It is interesting to note that in this convective ITCZ there was no sign of a nucleation or small-diameter Aitken mode being mixed down into the MBL from regions of cloud outflow [*Clarke et al.*, 1998] as has been routinely observed in the Pacific [*Clarke et al.*, 1998; *Covert et al.*, 1996].

The number size distributions in the two Southern Hemisphere marine air masses both had distinct Aitken and accumulation modes. The modes were larger in diameter and number than that measured in the Northern Hemisphere marine air mass presumably as a result

Table 1a. Aitken and Accumulation Mode Fit Parameters for the Dry (<10% RH) Number Size Distribution[a]

Air mass Regime	Aitken Mode N, cm^{-3}	Aitken Mode D_{gn}, nm	Aitken Mode σ_g	Accumulation Mode N,	Accumulation Mode D_{gn}, nm	Accumulation Mode σ_g
North America	490 ± 150	37 ± 3.2	1.37 ± 0.051	780 ± 230	160 ± 21	1.44 ± 0.046
NH marine	160 ± 42	30 ± 3.7	1.40 ± 0.026	58 ± 23	120 ± 22	1.59 ± 0.12
Dust	220 ± 55	39 ± 2.2	1.41 ± 0.057	180 ± 35	125 ± 9	1.52 ± 0.062
Mixed	230 ± 59	43 ± 4.9	1.48 ± 0.065	420 ± 120	140 ± 10	1.65 ± 0.10
Biomass burning	77 ± 73	47 ± 16	1.40 ± 0.12	480 ± 190	150 ± 12	1.63 ± 0.074
SH marine tropics	99 ± 37	44 ± 7.2	1.40 ± 0.067	100 ± 45	160 ± 19	1.54 ± 0.089
SH marine temperate	240 ± 170	41 ± 5.0	1.40 ± 0.059	140 ± 31	160 ± 15	1.37 ± 0.059

[a]Mean values plus or minus one standard deviation are given for each air mass regime.

Table 1b. Aitken and Accumulation Mode Fit Parameters for the Number Size Distribution at 55% RH[a]

Air mass Regime	Aitken Mode			Accumulation Mode		
	N, cm^{-3}	D_{gn}, nm	σ_g	N,	D_{gn}, nm	σ_g
North America	500 ± 140	40 ± 5.2	1.50 ± 0.077	580 ± 300	200 ± 23	1.45 ± 0.088
NH marine	180 ± 57	33 ± 6.2	1.50 ± 0.11	48 ± 18	150 ± 23	1.51 ± 0.12
Dust	240 ± 55	46 ± 4.5	1.42 ± 0.067	130 ± 20	150 ± 5	1.35 ± 0.048
Mixed	250 ± 59	56 ± 8.8	1.50 ± 0.021	410 ± 97	160 ± 17	1.64 ± 0.082
Biomass burning	170 ± 73	73 ± 16	1.65 ± 0.16	390 ± 150	190 ± 18	1.54 ± 0.061
SH marine tropics	100 ± 29	56 ± 10	1.50 ± 0.092	97 ± 41	220 ± 29	1.48 ± 0.084
SH marine temperate	210 ± 86	51 ± 4.2	1.46 ± 0.070	150 ± 29	210 ± 18	1.33 ± 0.046

[a]Mean values plus or minus one standard deviation are given for each air mass regime.

of longer MBL residence times (Figure 1), minimal precipitation (Figure 3), and large source of biogenic sulfur (Figure 7) available for condensational growth.

7. Conclusions

Meteorological data, calculated back trajectories, trace gas distributions, and aerosol chemical and physical data were used to define seven distinct MBL air mass regimes along the Aerosols99 cruise track across the Atlantic Ocean. The seven MBL regimes defined in this paper included a North American air mass that had been over the ocean for several days, a winter season NH marine air mass, an air mass passing over Africa containing mineral dust, an air mass passing over Africa containing the products of biomass burning, a mixed mineral dust/biomass burning air mass, a SH tropical marine air mass, and a SH summer season marine temperate air mass. Each air mass exhibited distinct physical and/or chemical aerosol properties as a result of aerosol source, transformation, and sink processes. The aerosol properties and trace gas concentrations within each regime, described in this paper and other papers in this special section, provide a data set to test chemical transport models and satellite retrieval algorithms. Further information about the cruise and available data sets can be found at http://saga.pmel.noaa.gov.

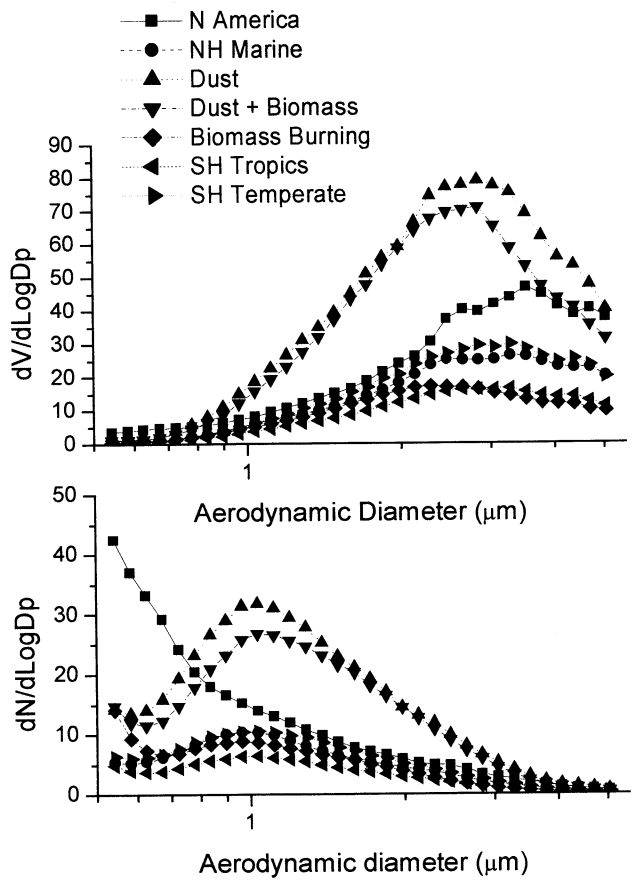

Figure 10. Regional average dry aerodynamic number and volume size distributions (APS data) in the seven air mass regimes along the Aerosols99 cruise track.

Acknowledgments. We thank the officers and crew of the NOAA RV *Ronald H. Brown* for their cooperation and support. This research was funded by the Aerosol Project of the NOAA Climate and Global Change Program, the NOAA Office of Oceanic and Atmospheric Research, and the NASA Global Aerosol Climatology Project. This is NOAA/PMEL contribution 2227 and JISAO contribution 778.

References

Andreae, M. O., Soot carbon and excess fine potassium: Long range transport of combustion derived aerosols, *Science, 220,* 1148–1151, 1983.

Andreae, M. O., W. Elbert, and S. J. de Mora, Biogenic sulfur emissions and aerosols over the tropical South Atlantic, 3, Atmospheric dimethylsulfide, aerosols, and cloud condensation nuclei, *J. Geophys. Res., 100,* 11,335–11,356, 1995.

Andreae, T. W., M. O. Andreae, and G. Schebeske, Biogenic sulfur emissions and aerosols over the tropical South Atlantic, 1, Dimethylsulfide in seawater and in the atmospheric boundary layer, *J. Geophys. Res., 99,* 22,819–22,829, 1994.

Andrés Hernández, M. D., J. Burkert, L. Reichert, J. P. Burrows, R. R. Dickerson, and B. Doddridge, Marine boundary layer peroxy radical chemistry during the Aerosols99 campaign: Measurements and analysis, *J. Geophys. Res.*, this issue.

Ayers, G. P., J. M. Cainey, H. Granek, and C. Leck, Dimethylsulfide oxidation and the ratio of methanesulfonate to non sea-salt sulfate in the marine aerosol, *J. Atmos. Chem., 25,* 307–325, 1996.

Bates, T. S., J. D. Cline, R. H. Gammon, and S. R. Kelly-Hansen, Regional and seasonal variations in the flux of oceanic dimethylsulfide to the atmosphere, *J. Geophys. Res., 92,* 2930–2938, 1987.

Bates, T. S., J. A. Calhoun, and P. K. Quinn, Variations in the methanesulfonate to sulfate molar ratio in submicrometer marine aerosol particles over the South Pacific Ocean, *J. Geophys. Res., 97,* 9859–9865, 1992.

Bates, T. S., R. P. Kiene, G. V. Wolfe, P. A. Matrai, F. P. Chavez, K. R. Buck, B. W. Blomquist, and R. L. Cuhel, Cycling of sulfur in surface seawater of the northeast Pacific, *J. Geophys. Res., 99,* 7835–7843, 1994.

Bates, T. S., B. J. Huebert, J. L. Gras, F. B. Griffiths, and P. A. Durkee, International Global Atmospheric Chemistry (IGAC) Project's First Aerosol Characterization Experiment (ACE 1): Overview, *J. Geophys. Res., 103,* 16,297–16,318, 1998a.

Bates, T. S., V. N. Kapustin, P. K. Quinn, D. S. Covert, D. J. Coffman, C. Mari, P. A. Durkee, W. De Bruyn, and E. Saltzman, Processes controlling the distribution of aerosol particles in the lower marine boundary layer during the First Aerosol Characterization Experiment (ACE 1), *J. Geophys. Res., 103,* 16,369–16,383, 1998b.

Bates, T. S., P. K. Quinn, D. S. Covert, D. J. Coffman, J. E. Johnson, and A. Wiedensohler, Aerosol physical properties and processes in the lower marine boundary layer: A comparison of shipboard sub-micron data from ACE 1 and ACE 2, *Tellus, 52,* 258–272, 2000.

Bergametti, G., L. Gomes, G. Coude-Gaussen, P. Rognon, and M.-N. Le Coustumer, African dust observed over Canary Islands: Source-regions identification and transport pattern for some summer situations, *J. Geophys. Res., 94,* 14,855–14,864, 1989.

Berner, A., C. Lurzer, F. Pohl, O. Preining, and P. Wagner, The size distribution of the urban aerosol in Vienna, *Sci. Total Environ., 13,* 245–261, 1979.

Cattell, F., W. Scott, and D. du Cros, Chemical composition of aerosol particles greater than 1-μm diameter in the vicinity of Tasmania, *J. Geophys. Res., 82,* 3457–3462, 1977.

Chameides, W. L., and A. W. Stelson, Aqueous-phase chemical processes in deliquescent sea-salt aerosols: A mechanism that couples the atmospheric cycles of S and sea salt, *J. Geophys. Res., 97,* 20,565–20,580, 1992.

Clarke, A. D., J. L. Varner, F. Eisele, R. L. Mauldin, D. Tanner, and M. Litchy, Particle production in the remote marine atmosphere: Cloud outflow and subsidence during ACE 1, *J. Geophys. Res., 103,* 16,397–16,409, 1998.

Covert, D. S., V. N. Kapustin, T. S. Bates, and P. K. Quinn, Physical properties of marine boundary layer aerosol particles of the mid-Pacific in relation to sources and meteorological transport, *J. Geophys. Res., 101,* 6919–6930, 1996.

Covert, D. S., A. Wiedensohler, and L. M. Russell, Particle charging and transmission efficiencies of aerosol charge neutralizers, *Aerosol Sci. Technol., 27,* 208–214, 1997.

Davis, D., et al., Dimethyl sulfide oxidation in the equatorial Pacific: Comparison of model simulations with field observations of DMS, SO_2, H_2SO_4(g), MSA(g), MS, and NSS, *J. Geophys. Res., 104,* 5765–5784, 1999.

Draxler, R. R., Hybrid Single-Particle Lagrangian Integrated Trajectories (HY-SPLIT): Version 3.0 user's guide and model description, *Tech. Rep. ERL ARL-195,* Natl. Oceanic and Atmos. Admin., Silver Spring, Md., 1992.

Feely, R. A., G. J. Massoth, and G. T. Lebon, Sampling of marine particulate matter and analysis by X-ray fluorescence spectrometry, in *Marine Particles: Analysis and Characterization, Geophys. Monogr. Ser.,* vol. 63, edited by D. C. Hurd and D. W. Spencer, pp. 251–257, AGU, Washington, D.C., 1991.

Feely, R. A., E. T. Baker, G. T. Lebon, J. F. Gendron, G. J. Massoth, and C. W. Mordy, Chemical variations of hydrothermal particles in the 1996 Gorda Ridge Event and chronic plumes, *Deep Sea Res., 45,* 2637–2664, 1998.

Fishman, J., and V. G. Brackett, The climatological distribution of tropospheric ozone derived from satellite measurements using version 7 Total Ozone Mapping Spectrometer and Stratospheric Aerosol and Gas Experiment data sets, *J. Geophys. Res., 102,* 19,275–19,278, 1997.

Gibb, S. W., R. Fauzi, C. Mantoura, and P. S. Liss, Ocean-atmosphere exchange and atmospheric speciation of ammonia and methylamines in the region of the NW Arabian Sea, *Global Biogeochem. Cycles, 13,* 161–178, 1999.

Gregoire, J.-M., S. Pinnock, E. Dwyer, and E. Janodet, Satellite monitoring of vegetation fires for EXPRESSO: Outline of activity and relative importance of the study area in the global picture of biomass burning, *J. Geophys. Res., 104,* 30,691–30,699, 1999.

Hoppel, W. A., G. M. Frick, and R. E. Larson, Effect of nonprecipitating clouds on the aerosol size distribution in the marine boundary layer, *Geophys. Res. Lett., 13,* 125–128, 1986.

Intergovernmental Panel on Climate Change (IPCC), *Climate Change 1995,* edited by J. T. Houghton et al., Cambridge Univ. Press, New York, 1996.

Keene, W. C., and J. L. Savoie, The pH of deliquesced sea-salt aerosol in polluted marine air, *Geophys. Res. Lett., 25,* 2181–2184, 1998.

Kiehl, J. T., T. L. Schneider, R. W. Portmann, and S. Solomon, Climate forcing due to tropospheric and stratospheric ozone, *J. Geophys. Res., 104,* 31,239–31,254, 1999.

King, M. D., Y. J. Kaufman, D. Tanre, and T. Nakajima, Remote sensing of tropospheric aerosols from space: Past, present, and future, *Bull. Am. Meteorol. Soc., 80,* 2229–2259, 1999.

Li-Jones, X., and J. M. Prospero, Variations in the size distribution of non-sea-salt sulfate aerosol in the marine boundary layer at Barbados: Impact of African dust, *J. Geophys. Res., 103,* 16,073–16,084, 1998.

Liss, P. S., and L. Merlivat, Air-sea gas exchange rates: introduction and synthesis, in *The Role of Air-Sea Exchange in Geochemical Cycling,* edited by P. Buat-Menard, pp. 113–127, D. Reidel, Norwell, Mass., 1986.

Liu, X., P. Van Espen, F. Adams, J. Cafmeyer, and W. Maenhaut, Biomass burning in Southern Africa: Individual particle characterization of atmospheric aerosols and savanna fire samples, *J. Atmos. Chem., 36,* 135–155, 2000.

Livingston, J.M., et al., Shipboard sunphotometer measurements of aerosol optical depth spectra and columnar water vapor during ACE-2 and comparison with selected land, ship, aircraft, and satellite measurements, *Tellus, 52,* 593–618, 2000.

Matthias-Maser, S., J. Brinkmann, and W. Schneider, The size distribution of marine atmospheric aerosol with regard to primary biological aerosol particles over the South Atlantic Ocean, *Atmos. Environ., 33,* 3569–3575, 1999.

Neusüss, C., D. Weise, W. Birmili, H. Wex, A. Wiedensohler, and D. S. Covert, Size-segregated chemical, gravimetric and number distribution-derived mass closure of the aerosol in Sagres, Portugal during ACE-2, *Tellus, 52,* 169–184, 2000.

O'Dowd, C. D., and M. H. Smith, Physico-chemical properties of aerosol over the northeast Atlantic: Evidence for wind speed related submicron sea-salt aerosol production, *J. Geophys. Res., 98,* 1137–1149, 1993.

Posfai, M., J. R. Anderson, P. Buseck, and H. Sievering,

Compositional variation of sea-salt mode aerosol particles from the North Atlantic, *J. Geophys. Res., 100,* 23,063–23,074, 1995.

Prospero, J. M., R. A. Glaccum, and R. T. Nees, Atmospheric transport of soil dust from Africa to South America, *Nature, 289,* 570–572, 1981.

Quinn, P. K., and D. J. Coffman, Local closure during ACE 1: Aerosol mass concentration and scattering and backscattering coefficients, *J. Geophys. Res., 103,* 16,575–16,596, 1998.

Quinn, P. K., T. S. Bates, J. E. Johnson, D. S. Covert, and R. J. Charlson, Interactions between the sulfur and reduced nitrogen cycles over the central Pacific Ocean, *J. Geophys. Res., 95,* 16,405–16,416, 1990.

Quinn, P. K., D. J. Coffman, V. N. Kapustin, T. S. Bates, and D. S. Covert, Aerosol optical properties in the marine boundary layer during ACE 1 and the underlying chemical and physical aerosol properties, *J. Geophys. Res., 103,* 16,547–16,563, 1998.

Quinn, P. K., T. S. Bates, D. J. Coffman, T. L. Miller, J. E. Johnson, D. S. Covert, J. P. Putaud, C. Neususs, and T. Novakov, A comparison of aerosol chemical and optical properties from the First and Second Aerosol Characterization Experiments, *Tellus, 52,* 238–257, 2000.

Quinn, P. K., D. J. Coffman, T. S. Bates, T. L. Miller, J. E. Johnson, K. Voss, E. J. Welton, and C. Neusüss, Dominant aerosol chemical components and their contribution to extinction during the Aerosols99 cruise across the Atlantic, *J. Geophys. Res.*, this issue.

Raes, F., Entrainment of free-tropospheric aerosol as a regulating mechanism for cloud condensation nuclei in the remote marine boundary layer, *J. Geophys. Res., 100,* 2893–2903, 1995.

Saltzman, E. S., D. L. Savoie, J. M. Prospero, and R. G. Zika, Methanesulfonic acid and non-sea-salt sulfate in Pacific air: Regional and seasonal variations, *J. Atmos. Chem., 4,* 227–240, 1986.

Sander, R., and P. J. Crutzen, Model study indicating halogen activation and ozone destruction in polluted air masses transported to the sea, *J. Geophys. Res., 101,* 9121–9138, 1996.

Savoie, D. L., J. M. Prospero, and E. S. Saltzman, Non-sea-salt sulfate and nitrate in trade wind aerosols at Barbados: Evidence for long-range transport, *J. Geophys. Res., 94,* 5069–5080, 1989.

Sievering, H., B. Lerner, J. Slavich, J. Anderson, M. Posfai, and J. Cainey, O_3 oxidation of SO_2 in sea-salt aerosol water: The size distribution of non-sea-salt sulfate during ACE 1, *J. Geophys. Res., 104,* 21,707–21,717, 1999.

Sokolik, I. N., and O. B. Toon, Incorporation of mineralogical composition into models of the radiative properties of mineral aerosol from UV to IR wavelengths, *J. Geophys. Res., 104,* 9423–9444, 1999.

Stratman, F., and A. Wiedensohler. A new data inversion algorithm for DMPS measurements, *J. Aerosol Sci., 27,* 339–340, 1997.

Thompson, A. M., and R. D. Hudson, Tropical tropospheric ozone (TTO) maps from Nimbus 7 and Earth Probe TOMS by the modified-residual method: Evaluation with sondes, ENSO signals, and trends from Atlantic regional time series, *J. Geophys. Res., 104,* 26,961–26,975, 1999.

Thompson, A. M., B. G. Doddridge, J. C. Witte, R. D. Hudson, W. T. Luke, J. E. Johnson, B. J. Johnson, S. J. Oltmans, and R. Weller, A tropical Atlantic paradox: Shipboard and satellite views of a tropospheric ozone maximum and wave-one in January–February 1999, *Geophys. Res. Lett., 27,* 3317–3320, 2000.

Turpin, B. J., J. J. Huntzicker, and S. V. Hering, Investigation of organic aerosol sampling artifacts in the Los Angeles Basin, *Atmos. Environ., 28,* 23,061–23,071, 1994.

Turpin, B. J., P. Saxena, and E. Andrews, Measuring and simulating particulate organics in the atmosphere: Problems and prospects, *Atmos. Environ., 34,* 2983–3013, 2000.

Van Dingenen, R., R. Raes, and N. R. Jensen, Evidence for anthropogenic impact on number concentration and sulfate content of cloud-processed aerosol particles over the North Atlantic, *J. Geophys. Res., 100,* 21,057–21,067, 1995.

Van Dingenen, R., A. O. Virkkula, F. Raes, T. S. Bates, and A. Wiedensohler, A simple non-linear analytical relationship between aerosol accumulation mode number and sub-micron volume, explaining their observed ratio in the clean and polluted marine boundary layer, *Tellus, 52,* 439–451, 2000.

Voss, K. J., E. J. Welton, J. E. Johnson, A. M. Thompson, P. K. Quinn, and H. Gordon, Lidar measurements during Aerosols99, *J. Geophys. Res.,* this issue (a).

Voss, K. J., E. Welton, P. Quinn, R. Frouin, and M. Reynolds, Aerosol optical depth measurements during the Aerosols99 experiment, *J. Geophys. Res.,* this issue (b).

Weber, R. J., P. H. McMurry, L. Mauldin, D. J. Tanner, F. L. Eisele, F. J. Brechtel, S. M. Kreidenweis, G. L. Kok, R. D. Schillawski, and D. Baumgardner, A study of new particle formation and growth involving biogenic trace gas species measured during ACE 1, *J. Geophys. Res., 104,* 21,673–21,684, 1999.

Wiedensohler, A., et al., Intercomparison study of the size-dependent counting efficiency of 26 condensation particle counters, *Aerosol Sci. Technol., 27,* 224–254, 1997.

Zhuang, L., and B. J. Huebert, Lagrangian analysis of the total ammonia budget during Atlantic Stratocumulus Transition Experiment/Marine Aerosol and Gas Exchange, *J. Geophys. Res., 101,* 4341–4350, 1996.

T. S. Bates (corresponding author) and P. K. Quinn, Pacific Marine Environmental Laboratory, NOAA, 7600 Sand Point Way NE, Seattle, WA 98115. (bates@pmel.noaa.gov)

D. J. Coffman, J. E. Johnson, and T. L. Miller, Joint Institute for the Study of the Atmosphere and Ocean, University of Washington, Seattle, WA 98195.

D. S. Covert, Department of Atmospheric Sciences, University of Washington, Seattle, WA 98195.

S. Leinert, C. Neusüss, A. Nowak, and A. Wiedensohler, Institute for Tropospheric Research, Permoserstr. 15, 04318 Leipzig, Germany.

(Received June 28, 2000; revised August 24, 2000; accepted September 1, 2000.)